Entropy-Slope Reconstruction from Late-Time Geometry in an MG-Unbiased Pipeline

Aiden B. Smith

Independent Researcher

(Dated: February 10, 2026)

Abstract

We report finalized results from the entropy submission-hardening pipeline using an MG-unbiased late-time geometry profile. The forward inversion reconstructs the apparent-horizon entropy-slope function $\mu(A)$ from Pantheon+, cosmic chronometers, and BAO while excluding GR-anchored growth, lensing, and full-shape closure terms from the primary posterior. For the real-data stage, the recovered slope is negative on average, $\langle d\log\mu/d\log A\rangle = -0.237 \pm 0.315$, with $P(d\log\mu/d\log A > 0) = 0.214$. The background posterior is broad but well sampled ($H_0 = 70.11^{+2.47}_{-2.43}$ km s^{-1} Mpc^{-1}, $\Omega_m = 0.297^{+0.058}_{-0.043}$, acceptance 0.337, minimum ESS $\approx$ 3995). Mapping-variant stress tests remain sub-dominant relative to posterior width: fixed-Ω_m and residual variants shift median $\log\mu$ by at most 0.021 and 0.015, while the curved-horizon variant gives the largest shift, 0.056 (RMS significance 0.291σ). Function-space distances strongly disfavor strict BH ($D^2_{\rm BH} = 1.68 \times 10^{-4}$) relative to fitted non-BH families (best $D^2 = 4.54 \times 10^{-8}$). Synthetic BH-closure calibration with 24 SBC realizations yields near-nominal $\log\mu$ coverage (68%: 0.944; 95%: 1.000) and low invalid-logprob rate (1.00×10^{-3}). These outputs provide a validated baseline for next-stage joint MG inference.

I. SCOPE

We reconstruct the horizon entropy-slope modifier

$$\mu(A) \equiv \frac{(dS/dA)_{\rm BH}}{dS/dA}, \tag{1}$$

with the forward apparent-horizon mapping implemented in the entropy pipeline. The analysis is the completed hardening run `entropy_submission_hardening_20260210_203502UTC`, with a real-data stage, robustness ablations, and synthetic closure calibration.

The real-data posterior uses the MG-unbiased profile: GR-anchored growth, lensing, and full-shape constraints are excluded from primary inference to reduce cross-sector GR-closure bias. Results therefore quantify the entropy slope required by late-time geometry channels under this mapping.

II. REAL-DATA RESULTS

A. Primary posterior

The real-data stage reports

$$H_0 = 70.11^{+2.47}_{-2.43}\ \mathrm{km\ s^{-1}Mpc^{-1}}, \tag{2}$$

$$\Omega_m = 0.297^{+0.058}_{-0.043}, \tag{3}$$

with acceptance fraction 0.337 and minimum effective sample size $\mathrm{ESS}_{\mathrm{min}} \approx 3995$.

The entropy-slope summaries are

$$\left\langle \frac{d\log\mu}{d\log A} \right\rangle = -0.23697 \pm 0.31483, \tag{4}$$

$$P\left(\frac{d\log\mu}{d\log A} > 0 \right) = 0.2143, \tag{5}$$

so $\sim 78.6\%$ posterior weight lies at negative slope. The area-averaged offset statistic is consistent with small net displacement,

$$\langle m \rangle = -0.0035 \pm 0.1523. \tag{6}$$

B. Mapping-variant robustness

Mapping stress tests are stable relative to posterior width. Relative to the baseline variant (V1_free), median-shape shifts are:

- V0_fixedOm: $\mathrm{RMS}(\Delta\mu/\sigma) = 0.080$, $\max|\Delta\log\mu| = 0.0214$.
- V2_residual: $\mathrm{RMS}(\Delta\mu/\sigma) = 0.062$, $\max|\Delta\log\mu| = 0.0153$.
- V1_curved: $\mathrm{RMS}(\Delta\mu/\sigma) = 0.291$, $\max|\Delta\log\mu| = 0.0562$.

The curved-horizon nuisance is the dominant mapping perturbation but remains sub-1σ in RMS significance.

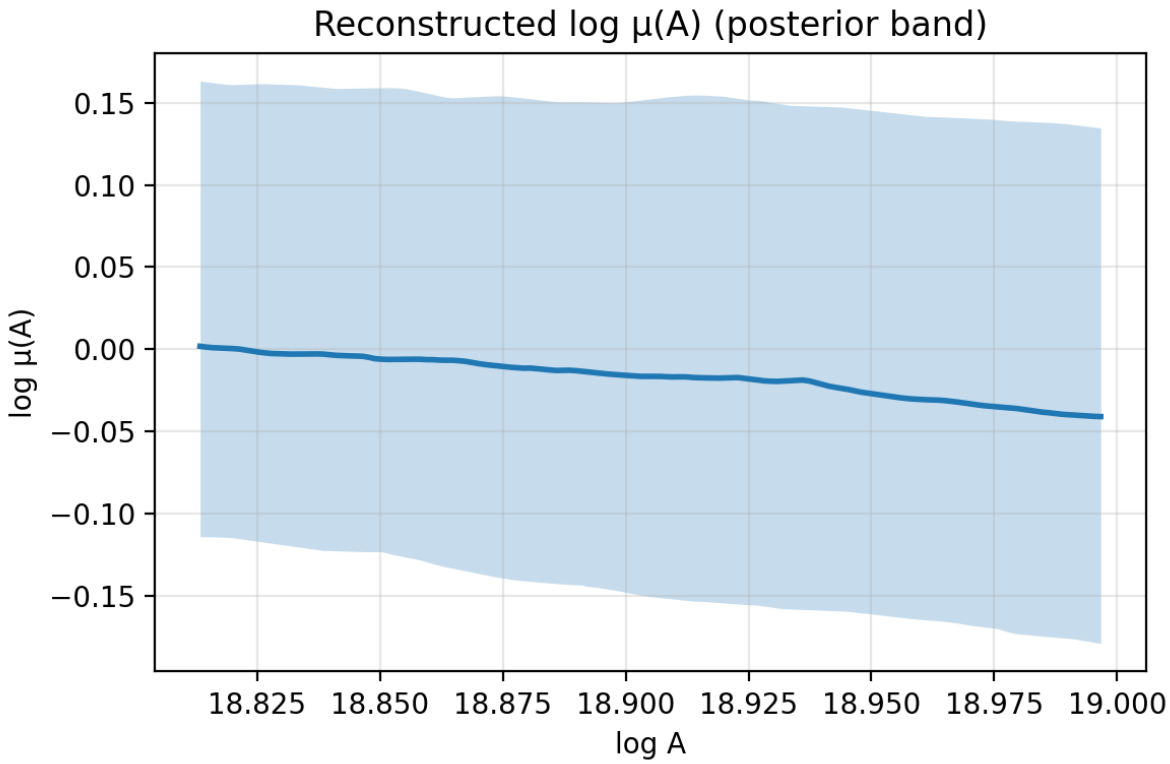

FIG. 1. Posterior band for $\log \mu(\log A)$ from the finalized MG-unbiased real-data stage.

C. Function-space proximity

Weighted function-space distances to parametric families (fit to posterior mean) are

$$\begin{aligned} D^2_{\rm BH} &= 1.68 \times 10^{-4}, \\ D^2_{\rm Tsallis} &= 4.54 \times 10^{-8}, \quad D^2_{\rm Barrow} = 4.54 \times 10^{-8}, \\ D^2_{\rm Kaniadakis} &= 1.12 \times 10^{-7}. \end{aligned} \tag{7}$$

In this run, non-BH families track the reconstructed shape much better than strict BH. Best-fit summary parameters are $\delta_{\rm Tsallis} = 1.23697$, $\Delta_{\rm Barrow} = 0.47393$, and $\tilde{\beta}_{\rm Kaniadakis} = 0.50660$.

III. ABLATION AND SYNTHETIC CLOSURE

A. Ablation suite

Seven ablation cases were executed (kernel, covariance, and smoothing variations). Across

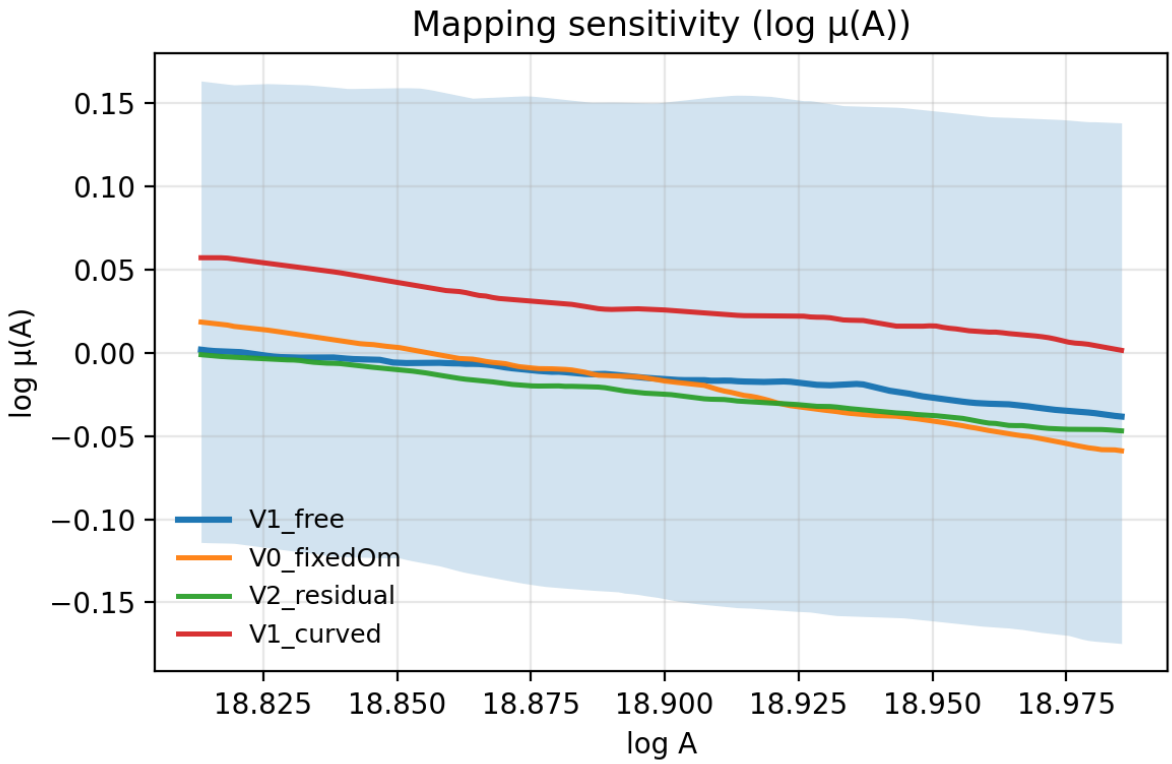

FIG. 2. Mapping-variant comparison of reconstructed $\log \mu(\log A)$.

cases,

$$D^2_{\mathrm{BH}} \in [0.117,\, 0.553], \qquad \min D^2_{\mathrm{Kaniadakis}} = 4.37 \times 10^{-3}. \tag{8}$$

The qualitative ordering is consistent with the real-data stage: non-BH families remain much closer than BH across tested settings.

B. Synthetic BH closure (SBC)

The synthetic closure stage completed $N = 24$ SBC realizations with BH truth. Coverage metrics are

$$\log \mu(x) : \; C_{68} = 0.944, \; C_{95} = 1.000, \tag{9}$$

$$\log \mu(\log A) : \; C_{68} = 0.940, \; C_{95} = 1.000, \tag{10}$$

$$H(z) \text{ pointwise} : \; C_{68} = 0.739, \; C_{95} = 0.981, \tag{11}$$

$$H(z) \text{ simultaneous} : \; C_{68} = 0.917, \; C_{95} = 0.958. \tag{12}$$

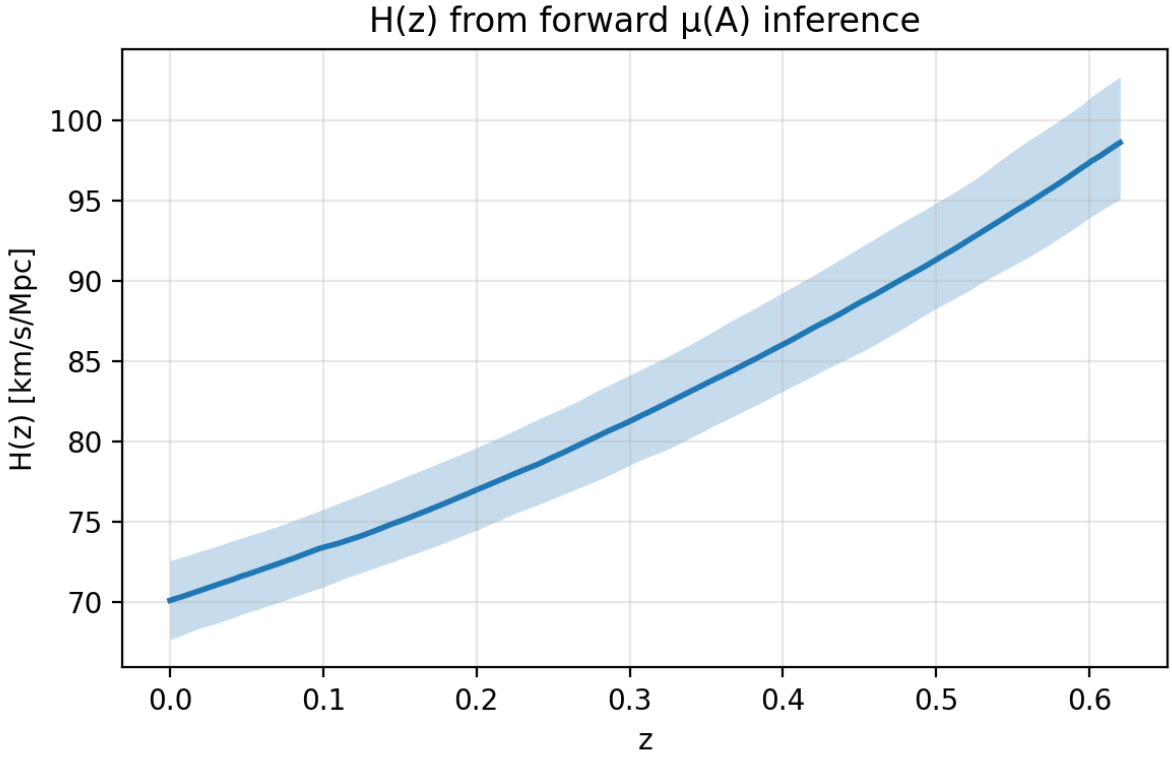

FIG. 3. Forward-reconstructed $H(z)$ band for the same posterior draws.

Sampler health remained stable. SBC acceptance was 0.3628 on average (p10/p50/p90 = 0.3589/0.3625/0.3693). The invalid-logprob rate was 1.00×10^{-3} (p90 1.53×10^{-3}; max 1.80×10^{-3}), dominated by prior-bound hits on $\log \sigma_{d2}$.

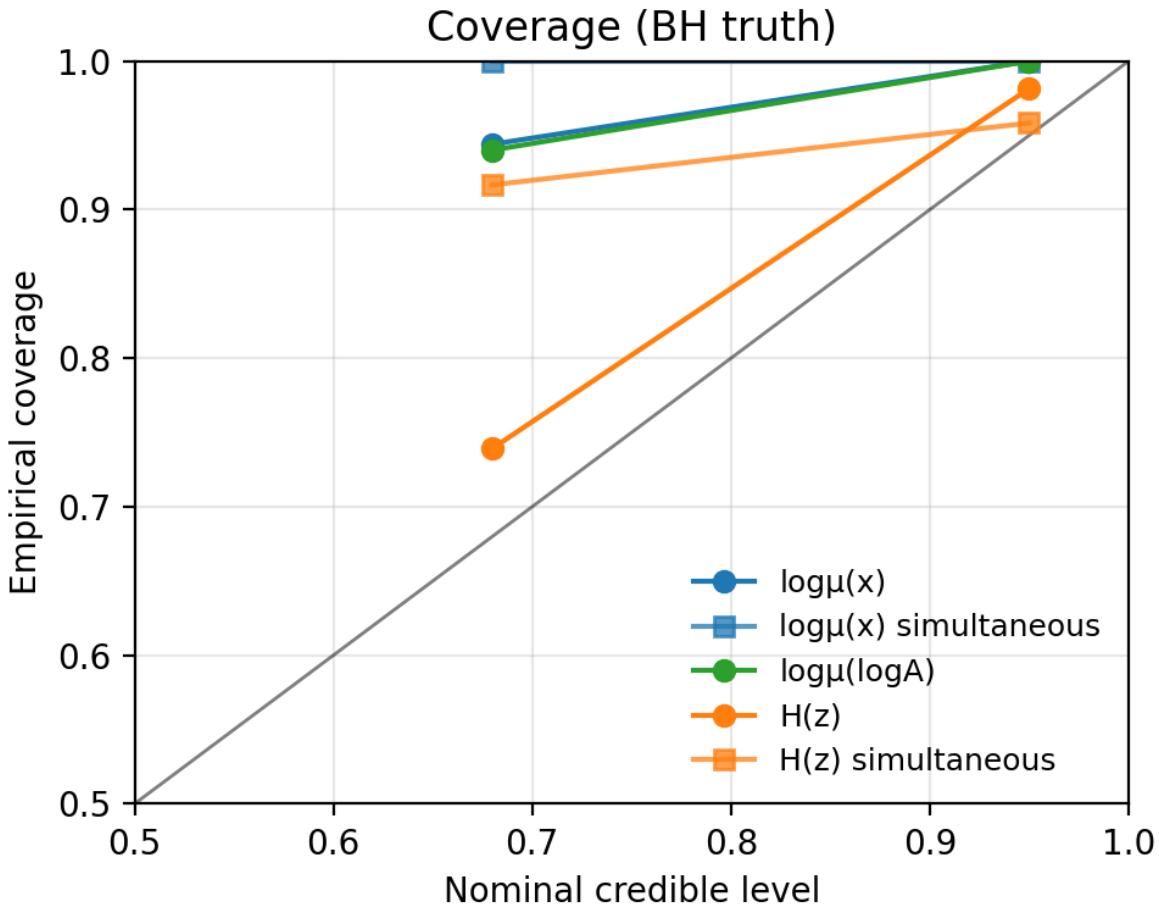

Figure: Synthetic-closure coverage summary from the BH-truth SBC stage.

IV. CONCLUSION

The hardening pipeline completed end-to-end and returns a consistent result: under the MG-unbiased geometry profile, the recovered entropy slope is mildly-to-moderately negative in posterior mean, with broad uncertainty but clear sign preference toward negative values. Mapping-variant shifts are limited, ablation behavior is qualitatively stable, and synthetic closure calibration is healthy enough to support next-stage joint analyses.

ACKNOWLEDGMENTS

This work used A.I. tools extensively, including ChatGPT 5.3.

DATA AVAILABILITY AND DOIS

- O3 modified-gravity tension anomaly repository (Zenodo): urlhttps://doi.org/10.5281/zenodo.18585598.
- O3 search-sensitivity injection data (Zenodo): urlhttps://doi.org/10.5281/zenodo.7890437.
- GWTC-3 catalog: urlhttps://doi.org/10.1103/PhysRevX.13.041039.
- Pantheon+ constraints: urlhttps://doi.org/10.3847/1538-4357/ac8e04.
- Planck 2018 parameters: urlhttps://doi.org/10.1051/0004-6361/201833910.
- Planck 2018 lensing: urlhttps://doi.org/10.1051/0004-6361/201833886.
- SDSS DR12 BAO: urlhttps://doi.org/10.1093/mnras/stx721.
- eBOSS DR16 constraints: urlhttps://doi.org/10.1103/PhysRevD.103.083533.
- DESI 2024 BAO constraints: urlhttps://doi.org/10.1088/1475-7516/2025/02/021.
- Cosmic-chronometer component DOI: urlhttps://doi.org/10.1088/1475-7516/2012/08/006.
- Cosmic-chronometer component DOI: urlhttps://doi.org/10.1103/PhysRevD.71.123001.
- Cosmic-chronometer component DOI: urlhttps://doi.org/10.1088/1475-7516/2010/02/008.